ACS APPLIED MATERIALS & INTERFACES

Research Article

Cite This: ACS Appl. Mater. Interfaces 2019, 11, 963−972

www.acsami.org

Sodium Superionic Conductors Based on Clusters

Hong Fang and Puru Jena*

Virginia Commonwealth University, Richmond, Virginia 23284, United States

ABSTRACT: Owing to the high abundance and low cost of sodium (Na), Na-based rechargeable batteries hold great potential for large-scale applications in the future energy industry. However, as key component of the battery electrolyte, only a few Na-based superionic conductors can reach the ionic conductivity comparable to that of liquid or gel electrolytes. Here, we provide a guideline for the development of cluster-based Na-rich antiperovskite superionic conductors using computational studies. With a selected cluster ion BCl_4^-, we are able to achieve high-room-temperature Na-ionic conductivity over 10^{-3} S/cm and low activation energies below 0.2 eV in the antiperovskite crystals $Na_3S(BCl_4)$ and $Na_3S(BCl_4)_{0.5}I_{0.5}$. In addition, these materials have large bandgaps and favorable mechanical properties. A comprehensive study of the stability and formation energy of these materials further illustrates possible routes for their synthesis. New insights into the conduction mechanism of these cluster-based superionic conductors are provided, including the cooperative motion of Na ions and the significant reduction of the migration barrier due to the changing orientation of the cluster ion.

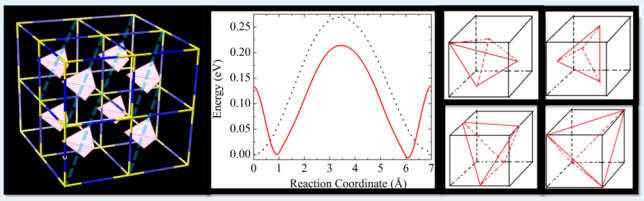

KEYWORDS: *solid electrolyte, sodium-ion battery, antiperovskite, superionic conductivity, low activation energy, quasi rigid unit modes, mechanical property*

INTRODUCTION

Sodium (Na) superionic conductors, exhibiting high Na-ionic conductivity in the solid state, are vital for the development of the next-generation Na ion batteries (SIB) that are cheaper, safer, more powerful, and have longer cycle life than those currently used.[1] However, among the known Na superionic conductors in the past three decades, only a few can reach an ionic conductivity of the order of 10^{-3} S/cm at room temperature (RT) that is comparable to that of the liquid or gel electrolytes. These include the selenide-based electrolyte Na_3PSe_4,[2] sodium β''-alumina ceramic electrolyte,[3] NASICON electrolyte $Na_3Zr_2Si_2PO_{12}$,[4] Na-glass electrolyte $Na_{2.99}Ba_{0.005}OCl_{1-x}(OH)_x$,[5] polyborate salt electrolyte $NaCB_9H_{10}$,[6] and the most recent $Na_{11}Sn_2PS_{12}$.[7]

Development of solids with enhanced ionic conductivities is urgent and in great need, as demonstrated by recent works on a wide range of Na and lithium (Li) superionic conductors.[8−17] Among these, Li/Na-rich antiperovskite family, exemplified by Li_3OBr and Na_3OBr, show potential as solid electrolytes due to their structural tolerance and superionic conductivity.[18−21] Most recent study of the Li-rich antiperovskites shows that the ionic conductivity can be greatly enhanced by using cluster ions to replace elemental halogens inside the material.[22] High RT conductivity of Li of the order of 10^{-2} S/cm and low activation energy below 0.25 eV are expected to be achieved with selected cluster ion, such as BF_4^-, which has large size and proper internal charge distribution. The ionic conductivity is found to be positively related to the vibrational modes of the cluster ions as near-rigid bodies, i.e., the so-called quasi rigid unit modes (qRUMs) in the materials' phonon spectra. Mixing the cluster ion with the elementary halogen in the Li-rich antiperovskites can further boost the RT ionic conductivity, due to the large size difference between the cluster ion and the elementary ion.

On the other hand, the RT ionic conductivity in the Na-rich antiperovskites is rather low, only of the order of 10^{-8} S/cm in Na_3OBr.[18−21] Although it seems natural to think of applying the same strategy, as has been done for Li-rich antiperovskites, to boost the ionic conductivity of the material by using cluster ions, incorporation of cluster ions such as CN^-, BH_4^-, and BF_4^- in the Na-rich antiperovskites has shown limited effect on improving their conductive properties.[19] The experimental activation energies of Na_3OX (X = Cl or Br) are around 0.7 eV,[18−21] which is much higher than the regular value below 0.3 eV. The calculated Young's modulus of the sodium antiperovskites is above 50 GPa with Poisson's ratio around 0.22.[23] These values correspond to ceramics-like materials, which makes them hard to densify as electrolytes having close contact with electrodes.

Here, bearing in mind the difference between Na and Li, we establish, by using cluster ions, a guideline for the design of new Na-rich antiperovskites with high RT superionic conductivity and low activation energy. According to our computational study, the as-developed crystals can reach a RT ionic conductivity of 10^{-3} S/cm and low activation energies (<0.20 eV). They also show large bandgap (~4.0 eV) and favorable mechanical properties. Through a side-by-side study with Na_3OBr, the stability, possible synthetic routes, and conduction mechanism of the cluster-based Na-rich antiperovskites are also provided.

Received: October 30, 2018
Accepted: December 14, 2018
Published: December 14, 2018

DOI: 10.1021/acsami.8b19003
ACS Appl. Mater. Interfaces 2019, 11, 963−972

Table 1. Calculated Goldschmidt's Tolerance Factor, $t = (r_B + r_{Na})/\sqrt{2}(r_A + r_{Na})$, of the Studied Na-Rich Antiperovskite Structures, where r_A, r_B, and r_{Na} are the Ionic Radii of the Divalent Anion, Monovalent Anion, and Na, Respectively[a]

crystal	BL (Å)	r (Å)	t	LP (Å)	CS (Å^3/unit cell)	V_{Na}/CS[b]
Na_3OBr		1.82	0.87	4.57[c]	68.92	0.28
$Na_3O(BF_4)$	1.41	2.43	1.05	4.74	76.03	0.26
$Na_3O(AlH_4)$	1.62	2.57	1.09	4.74	71.98	0.27
$Na_3S(BCl_4)$	1.85	3.29	1.10	5.88	127.89	0.15
$Na_{2.875}S(BCl_4)$[d]	1.85	3.29	1.10	5.96	136.30	0.14(4)
$Na_{2.875}S(BCl_4)_{0.5}I_{0.5}$[d]	1.85	2.67[e]	0.95	5.72	137.26	0.14(3)

[a]The ionic radii of B, Al, Li, Na, O, S, Br, and I are 0.41, 0.67, 0.90, 1.16, 1.26, 1.70, 1.82, and 2.06 Å, respectively. BL is the bond length inside the cluster ion. In each case, the channel size (CS) is calculated by using the volume of the unit cell minus the volumes of all of the ions (apart from Na ions) inside. The volume of a cluster ion is defined as the volume of the cube enclosing the cluster. The volume of the unit cell is computed from the optimized lattice parameter (LP) of the material with pseudo-cubic symmetry. V_{Na}/CS is the ratio between the total volume of the three Na atoms inside a unit cell vs the channel size that is available for Na to migrate in each material. [b]These values are compared to that of V_{Li}/CS = 0.15 for $Li_3S(BF_4)$. [c]Experimental value.[9] [d]Nonstoichiometric system with one Na^+ vacancy in a 2 × 2 × 2 supercell used in the simulations. [e]Calculated as the average of ionic radii of I^- and BCl_4^-.

Na-Rich Antiperovskites Based on Cluster Ions. We started replacing Br in Na_3OBr with several cluster ions such as AlH_4^-, BF_4^-, and BCl_4^-, whose vertical detachment energies, the energy needed to remove one electron from the anion without changing its geometry, are larger than that of Cl^-. These superhalogen clusters are chosen because, when forming the antiperovskite structures Na_3BA (A = cluster; B = O or S), their ionic radii result in tolerance factors that fall in the ideal range of 0.813−1.107,[24] as shown in Table 1. We note that the use of sulfur instead of oxygen to couple with the cluster ion BCl_4^- is important to generate the proper tolerance factor. The suitability of cluster ions is then further screened using the following criteria: in terms of its potential to enable the highest ionic conductivity in the material, the chosen cluster ion should have proper size and internal charge distribution to produce large channel size (CS) in the antiperovskite. The channel size measures the free space available for Na^+ to migrate and is calculated as the volume of the unit cell minus the volume occupied by ions other than Na^+. Also, as mentioned at the beginning, it has been found that the ionic conductivity in cluster-based materials is akin to a set of low-energetic phonon modes known as qRUMs.[22] The corresponding vibrations of the cluster can shift and alter the potential surface felt by the metal ions inside the material and facilitate the hopping by reducing the potential barrier.

As shown in Table 1, among the three candidates of cluster ions, BCl_4^- creates the largest channel size inside the material $Na_3S(BCl_4)$. This is due to the large size and the highly negative charge distribution on each Cl of BCl_4^-, making exceptionally large unit cell to reduce the repulsion between the cluster ion and sulfur. A similar case was observed in the study of Li-rich antiperovskite $Li_3S(BF_4)$, where the highly electronegative F in BF_4^- created a large channel size.[22] However, for a Na-based superionic conductor to reach a similar ionic conductivity as in the Li-based systems, one must take into account the larger size of Na^+ compared to Li^+. In this regard, a ratio of the volume of the metal ion (V_{Li} or V_{Na}) vs the channel size (CS) is a more reasonable yard stick than the channel size itself. For $Li_3S(BF_4)$ whose RT ionic conductivity is above 10^{-3} S/cm, the ratio of V_{Li}/CS is about 0.15. Among the three Na-rich antiperovskites in the current study, $Na_3S(BCl_4)$ has the same ratio of V_{Na}/CS = 0.15, whereas the other two have much larger values, 0.26 and 0.27 for $Na_3O(BF_4)$ and $Na_3O(AlH_4)$, respectively. These values are compared to the even larger value of 0.28 in Na_3OBr. It is obvious that smaller the ratio, higher ionic conductivity is likely to be achieved in the material. Thus, BCl_4^- and hence $Na_3S(BCl_4)$ are expected to produce the best performance of ionic conduction among the cluster-based Na-rich antiperovskites.

Given the nonspherical nature of the cluster ions, the optimized structures of $Na_3O(AlH_4)$, $Na_3O(BF_4)$, and $Na_3S(BCl_4)$ are pseudo-cubic with lattice parameters of 4.74, 4.74, and 5.88 Å, respectively, and angles close to 90°. In their ground state, all of the tetrahedral cluster ions, AlH_4^-, BF_4^-, and BCl_4^-, together with the cube, adopt a C_{3v} symmetry with one of the 3-fold axes of the tetrahedron along the diagonal of the pseudo-cubic cell, as shown in Figure 1. The Coulombic

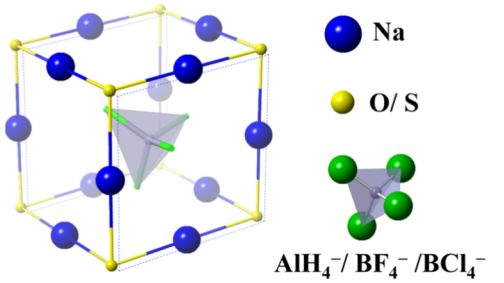

Figure 1. Optimized pesudo-cubic structures of $Na_3O(AlH_4)$, $Na_3O(BF_4)$, and $Na_3S(BCl_4)$ with cluster ions AlH_4^-, BF_4^-, and BCl_4^-, respectively. The tetrahedral cluster with the cube adopts a C_{3v} symmetry in the ground state, where the 3-fold axis of the tetrahedral unit is along the diagonal of the pseudo-cubic cell.

interaction created by the cluster units on each Na^+ ion is related to the orientation of the cluster ion inside the pseudo-cubic cell. Due to thermal excitation, the orientation of the cluster ion is expected to deviate from its ground state. It has been found that upon changing the orientation from the ground state, the Coulombic attraction from the cluster to the metal ion can reduce significantly, above the order of 0.01 eV/metal atom.[22,25]

All three studied Na-rich antiperovskites are confirmed to be lattice dynamically stable, as shown by their phonon spectra in Figure 2a, which are free of imaginary mode. From $Na_3O(AlH_4)$ and $Na_3O(BF_4)$ to $Na_3S(BCl_4)$, the phonons are greatly densified toward low energy and the spectral range is reduced by two-thirds, from (0−60 THz) in $Na_3O(AlH_4)$ to (0−20 THz) in $Na_3S(BCl_4)$. It is found that $Na_3S(BCl_4)$ has a set of qRUMs with an upper-bound energy as low as 2.5 THz

DOI: 10.1021/acsami.8b19003
ACS Appl. Mater. Interfaces 2019, 11, 963−972

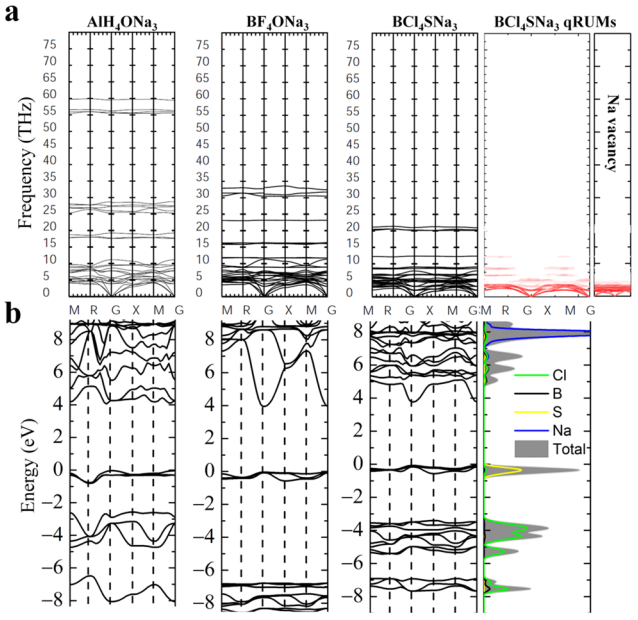

Figure 2. Calculated (a) phonon spectra and (b) electronic structures of $Na_3O(AlH_4)$, $Na_3O(BF_4)$, and $Na_3S(BCl_4)$. The qRUMs of $Na_3S(BCl_4)$ with the low energy are shown in red. qRUMs of a 2 × 2 × 2 $Na_3S(BCl_4)$ supercell with one Na^+ vacancy are also given. In such a case, the qRUMs are all densified to frequencies well below 5 THz. Electronic (partial) densities of states of $Na_3S(BCl_4)$ are also given.

(∼10 meV). This suggests that a great amount of vibrations of BCl_4^- units as near-rigid bodies can be excited at low and medium temperatures (RT ∼25 meV). The presence of qRUMs with ultralow energy suggests a reduced overall attraction between the anionic cluster and Na^+ compared to the other materials and is consistent with the exceptionally large channel size and small V_{Na}/CS ratio, making it easy for both Na^+ and the cluster BCl_4^- to move inside the lattice.

Stability and Possible Synthesis Routes. Having established that BCl_4^- is likely to be a good choice, we further test the stability of $Na_3S(BCl_4)$ by carrying out molecular dynamics simulations on the material at high temperatures. After allowing both the lattice and ionic positions to fully relax over 100 ps with constant temperature and pressure, no sign of phase transition and/or disorder is discovered. Figure 3a shows the calculated pair distribution function of the material by using the simulation data at 400 and 600 K, suggesting that the phase is maintained at these high temperatures. To show that the studied material remains vibrationally stable, we calculate the position correlation function,[26,27] defined as

$$p(t) = \langle [r_i(t + t_0) - R_i] \cdot [r_i(t_0) - R_i] \rangle \quad (1)$$

R_i is the thermal average position of the ith ion in the crystal. r_i is the position of the ion at a given time. The average is taken over time origins t_0 and number of ions of the same species. If the studied ions are vibrationally stable, the calculated function should be zero when $t \rightarrow \infty$, since the displacements at long time interval become uncorrelated. Figure 3b shows the calculated position correlation function for ions other than sodium at 600 K. The fluctuation around zero at large t suggests that the elements are vibrationally stable. Also shown is the calculated time-dependent mean square displacement (MSD)

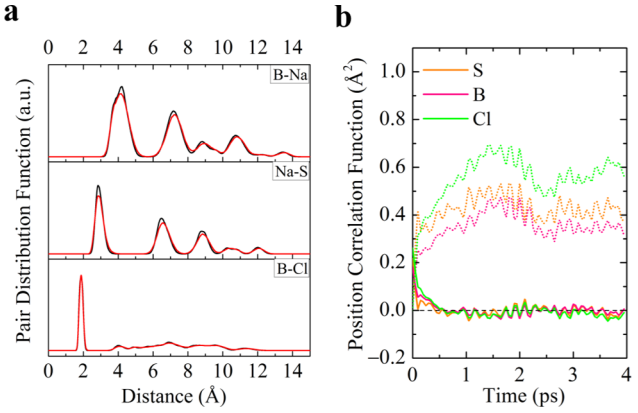

Figure 3. (a) Calculated pair distribution functions of $Na_3S(BCl_4)$ at simulated 400 K (black) and 600 K (red). The structure of the material is stable with slightly broadened peaks at high temperature. (b) Calculated position correlation functions (solid lines) and mean square displacements (dotted lines) for S, B, and Cl at 600 K. The position correlation functions fluctuate toward zero when $t \rightarrow \infty$, suggesting that the phase is vibrationally stable. The mean square displacement for each element fluctuates around a constant value which is twice the value of the corresponding position correlation function at $t = 0$, suggesting that there is no superionic conduction of these elements inside the material.

$$\Delta r(t)^2 = \langle [r_i(t + t_0) - r_i(t_0)]^2 \rangle \quad (2)$$

which suggests that there is no diffusion of these ions.

To study the formation energy of $Na_3S(BCl_4)$, we collected all of the crystals whose structures are available in material database (e.g., ICSD and COD) containing the four elements Na, S, B, and Cl. These include, ranked in descending order of their calculated energy (eV) per atom (value in parenthesis), Na metal (−1.307), Na_2S (−3.325), NaSH (−3.623), Na_2S_4 (−3.774), $NaBCl_4$ (−3.789), Na_2S_5 (−3.820), BNa_3S_3 (−4.242), $B_2Na_2S_5$ (−4.775), $B_3Na_3S_6$ (−4.846), and NaB_6Cl_6 (−4.939). It is known that $NaBCl_4$ can be obtained from the thermolysis of $NaB(O_3SCl_4) \rightarrow SO_3 + NaBCl_4$.[28] However, the crystal structure of $NaBCl_4$ is unavailable. The calculated energy here for $NaBCl_4$ is based on the crystal structure of $NaBF_4$. The calculated energy of $Na_3S(BCl_4)$ is −3.594 eV/atom. Only those materials (i.e., Na metal, Na_2S, NaSH, and $NaBCl_4$ in the above list) whose energies are higher than or close to this value (−3.594 eV/atom) are likely to result in low formation energy when they serve as reactants to produce $Na_3S(BCl_4)$. For instance, NaB_6Cl_6 having much lower energy than that of $Na_3S(BCl_4)$ cannot be an ideal reactant, since $B_6Cl_6^-$ is a very stable octahedral cluster and therefore hard to break to form the BCl_4^- unit. It is found that the formation energy of $Na_3S(BCl_4)$ from the reaction $Na_2S + Na(BCl_4) \rightarrow Na_3S(BCl_4)$ is a positive value of 40.3 meV/atom. This is not ideal compared to the negative formation energy of Na_3OBr from a similar reaction $Na_2O + NaBr \rightarrow Na_3OBr$.

Another possible way is to use both Na metal and NaSH as reactants whose energies are higher than or similar to those of Na_2S and $Na_3S(BCl_4)$. Indeed, the calculated formation energy of $Na_3S(BCl_4)$ from the reaction $Na + NaSH + Na(BCl_4) \rightarrow Na_3S(BCl_4) + (1/2)H_2$ is negative (−82.4 meV/atom), suggesting a preferred route for synthesis. In fact, Na_3OX (X = halogen) has been successfully synthesized using a similar reaction of $NaOH + NaX + Na \rightarrow Na_3OX + (1/2)H_2$ involving Na metal.[18] NaX (X = halogen) and NaOH are

DOI: 10.1021/acsami.8b19003
ACS Appl. Mater. Interfaces 2019, 11, 963−972

first ground together in inert gas atmosphere. Then, the resulting powder is paved on Na metal and heated beyond the melting point of Na metal under vacuum to complete the reaction.[18] Similarly, we reckon that in the case of $Na_3S(BCl_4)$ after obtaining $Na(BCl_4)$ from the thermolysis of NaB-(O_3SCl_4), $Na(BCl_4)$ and NaSH can be ground together and paved on Na metal and heated in vacuum for the reaction to take place. Note that the Na/S ratio of NaSH is less than that of Na_2S. Therefore, depending on the completeness of the proposed reaction with Na, it is possible to introduce Na vacancies, which is vital to the superionic conductivity in the produced $Na_3S(BCl_4)$.[18−21]

Electronic Properties and Ionic Conductivity. The calculated band structures of $Na_3O(AlH_4)$, $Na_3O(BF_4)$, and $Na_3S(BCl_4)$ using density functional theory (DFT) with HSE06 functional are given in Figure 2b. The bandgaps, also seen as the upper limit of the electrochemical stability window of a solid electrolyte, are all about 4.0 eV, which are typical of a solid electrolyte in SIB[29] and similar to those of Na_3OX (X = halogen).[23] The valence and conduction band edges arise from the contribution of oxgen/sulfur (*p*-functions) and the cluster ions, respectively. The edges of $Na_3S(BCl_4)$ are quite flat, suggesting large effective masses of carriers and low electronic conductivity of the material, which is preferred for an electrolyte.

Ab initio molecular dynamics (AIMD) simulations are carried out to study the Na^+ conductivity of the materials. For Na_3OX (X = halogen), it has been reported that Na vacancy is most likely to form and is necessary for the superionic conductivity of the materials.[18,20] Indeed, according to our own simulations, no Na^+ conductivity is observed without the presence of at least one Na vacancy in the supercell, suggesting that Na^+ is not likely to conduct through hopping into the interstitial sites in these materials. For the cluster-based antiperovskites, we find that the Na vacancy is again necessary for the superionic conductivity. The calculated formation energy of one Na vacancy in a 2 × 2 × 2 supercell of $Na_3S(BCl_4)$ is 0.114 eV/sodium, slightly lower than the value of 0.115 eV/sodium of Na_3OBr.

Figure 4a shows the supercell used in our simulations, where one Na^+ vacancy is introduced to trigger fast-ion hopping. As shown in Table 1, with the presence of Na^+ vacancy, the channel size becomes significantly larger, and the ratio of V_{Na}/CS becomes smaller than that in the stoichiometric system. These factors can improve the ionic conduction. The calculated qRUMs of such system are given in Figure 2a. Compared to the perfect crystal, the qRUMs of the supercell with one Na^+ vacancy become nondegenerate and softened to frequencies well below 5 THz. This is expected since the presence of vacancy reduces the symmetry and provides more space for the clusters to move. In Figure 4c, we first obtain the diffusion coefficients of the materials from the averaged mean square displacement (MSD) of Na^+ extracted from the AIMD data collected over 250 ps after reaching thermal equilibrium. The Na^+ conductivity (σ) in each case is calculated from the Nernst−Einstein relation (see Method section), and RT conductivity is extrapolated by the Arrhenius relation (see eq m3 in the Method section for detail)

$$\sigma = \frac{A}{T}\exp\left(\frac{E_a}{kT}\right) \quad (3)$$

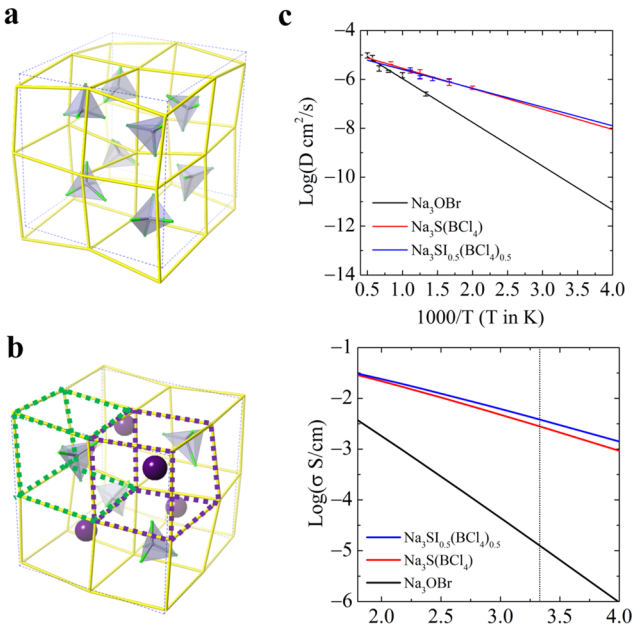

Figure 4. Snapshots of (a) $Na_3S(BCl_4)$ and (b) $Na_3S(BCl_4)_{0.5}I_{0.5}$ containing one Na^+ vacancy after 250 ps of AIMD simulations. BCl_4^- clusters are gray tetrahedra with Cl in green. Iodine atoms are in purple. Sulfur atoms are shown in yellow bonds. Sodium atoms are neglected for clarity. The supercell can be equipartitioned into unit cells containing either BCl_4^- or I^-, as shown by the green outline and the purple outline, respectively. (c) The calculated Na diffusion coefficients and conductivities of Na_3OBr, $Na_3S(BCl_4)$, and $Na_3S-(BCl_4)_{0.5}I_{0.5}$. The error of the diffusion coefficient (D) is transferred from the error of the slope of the linear fitting to the MSD data. The error of the logarithm of D is then estimated by $\log(D + \Delta D) = \log[D(1 + \Delta D/D)] \approx \log \Delta D + \Delta D/D$. $Na_3S(BCl_4)$ and $Na_3S-(BCl_4)_{0.5}I_{0.5}$ exhibit much higher conductivities and lower activation energies than that of Na_3OBr. The dotted line shows the ionic conductivity at room temperature.

As a benchmark, we first study the Na^+ conductivity of Na_3OBr. In the supercell, the calculated migration barrier from one Na site to the nearest vertex of ONa_6 octahedron (vacancy) using the nudged elastic band (NEB) method is about 0.33 eV, which agrees well with the former calculations using the same method.[18,20] Such value is much lower than the experimental value around 0.7 eV. There are two possible sources for this large discrepancy. One is the neglect of the vacancy formation energy (in the order of 0.2 eV) in the theoretical model. The other is the presence of grain boundaries inside the polycrystalline samples used in the experiments.[18,20] It has been proved recently that grain boundaries can significantly increase (in the order of 0.2 eV) the activation energy of antiperovskite superionic conductors and reduce the ionic conductivity by as much as several orders of magnitude.[30] Therefore, to achieve theoretical values to compare with experiments, it is important to intentionally introduce Na vacancies in the sample through, for example, Na depletion or doping of divalent alkali-earth metal ions.[18,20] It is also important to reduce grain boundaries inside the polycrystalline sample by increasing the grain size. It has been found that a sample with grain size larger than 400 nm in diameter can maintain about 85% of the theoretical ionic conductivity.[30] AIMD simulations are carried out for Na_3OBr at 750, 1000, 1250, 1500, 1750, and 2000 K. The calculated activation energy is 0.35 eV, in good agreement with the NEB

DOI: 10.1021/acsami.8b19003
ACS Appl. Mater. Interfaces 2019, 11, 963−972

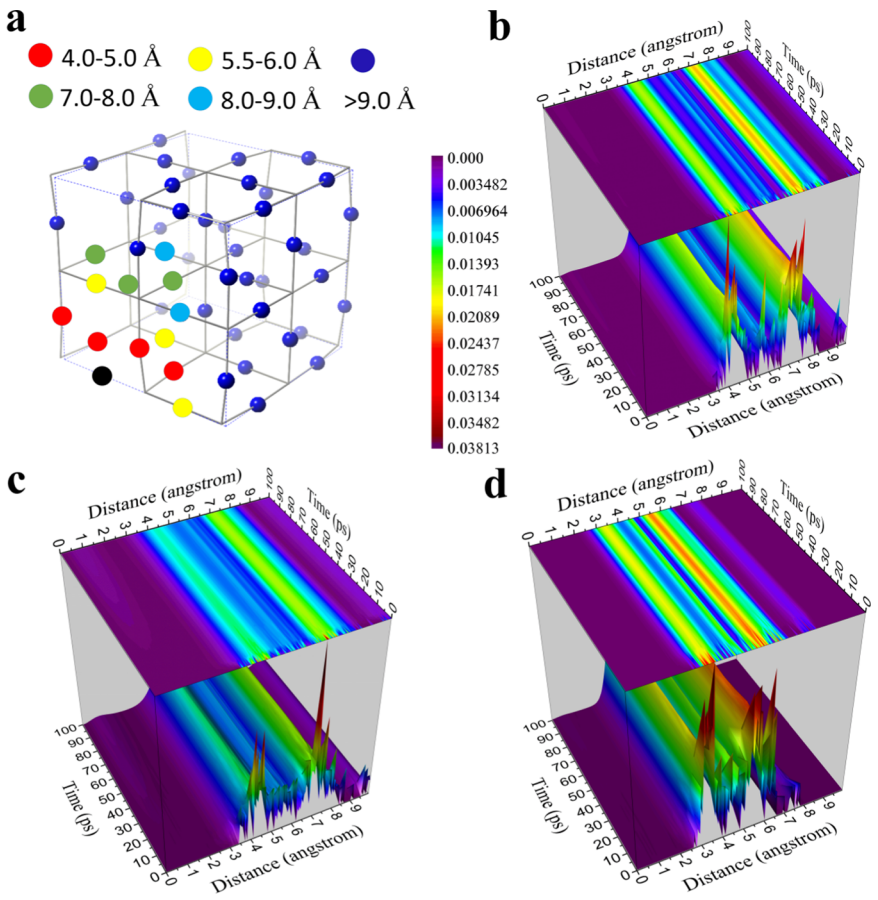

Figure 5. (a) Distances between Na−Na ion pairs in the crystal structure of $Na_3S(BCl_4)$. Computed distinct van Hove time correlation function and its projection on the "time−distance" plane for $Na_3S(BCl_4)$ at (b) 600 K and (c) 1200 K. (d) Calculated distinct van Hove time correlation function of Na_3OBr at 1200 K. The values of the time correlation function are normalized for comparison. Distinctive peaks of probability around Na−Na distances as those in the crystal structure in (a) are maintained throughout the time, suggesting a cooperative motion of Na^+ inside the materials.

computed value, suggesting that good convergence is reached in each simulation. The calculated conductivity of Na_3OBr at different temperatures is shown in Figure 4c.

Among the studied cluster-based Na-rich antiperovskites, $Na_3S(BCl_4)$, as expected, shows much higher Na^+ conductivity than the others. $Na_3O(BF_4)$ and $Na_3O(AlH_4)$ do not show ionic conductivities significantly higher than that of Na_3OBr. $Na_3O(AlH_4)$ also exhibits fast-ion migration of hydrogen at high temperatures, suggesting instability of AlH_4^- upon thermal excitation. AIMD simulations are carried out for $Na_3S(BCl_4)$ at 500, 600, 800, 900, and 1200 K. The calculated diffusion coefficient and ionic conductivity of $Na_3S(BCl_4)$ are shown in Figure 4c. The material exhibits a three-dimensional Na^+ conductivity of 2.8×10^{-3} S/cm at RT, which is significantly higher that of Na_3OBr (1.2×10^{-5} S/cm). The obtained activation energy (E_a) is 0.17 eV, which is much lower than that of Na_3OBr (0.35 eV), and is considered as low among the known sodium solid electrolytes.[29] We also calculated the migration barrier of Na^+ in $Na_3S(BCl_4)$ using the NEB method. Unlike Na_3OBr, given the orientational symmetry of BCl_4^- in the pseudo-cubic cell, there are 12 inequivalent routes for Na^+ to migrate between different vertices of the SNa_6 octahedron. After performing NEB calculation for each route, the averaged profile of energy barrier is obtained. It is found that the migration barrier is about 0.28 eV, which is significantly higher than the value (0.17 eV) obtained from the AIMD simulations. This indicates the importance of motions of the cluster ions, corresponding to the qRUMs, to the superionic properties of these materials. We will discuss this further in the section Conduction Mechanism.

One can further increase the Na^+ conductivity of the material by co-mixing the cluster ion with elementary halogen inside the antiperovskite lattice, making $Na_3S(BCl_4)_{1-x}A_x$ (A = Cl, Br or I; $0 < x < 1$). The mechanism is due to the following size effect. When the lattice accommodates the large cluster ion, it gives the elementary ions redundant space, which can serve as additional channel space for Na^+ to move around, hence enhancing the ionic conductivity of the material. As a result, larger the difference between the sizes of the cluster ion and the elementary ion, larger is the redundant space one can create. Consequently, higher Na^+ conductivity is likely to be achieved. We demonstrate this by using $Na_3S(BCl_4)_{0.5}I_{0.5}$ in Figure 4b. The calculated channel size and the ratio of V_{Na}/CS for the material are more favorable than those of $Na_3S(BCl_4)$, as shown in Table 1. From AIMD simulations at 600, 700, 800, and 900 K, the Na^+ diffusion coefficient and conductivity of the material are obtained; the results are given in Figure 4c. The extrapolated RT conductivity, 3.8×10^{-3} S/cm, of the mixed phase is indeed higher than (2.8×10^{-3} S/cm) of $Na_3S(BCl_4)$. The activation energy (0.15 eV) of $Na_3S(BCl_4)_{0.5}I_{0.5}$ is also significantly lower. Since iodine (I) has the largest size among halogens, it is expected that the Na^+

DOI: 10.1021/acsami.8b19003
ACS Appl. Mater. Interfaces 2019, 11, 963−972

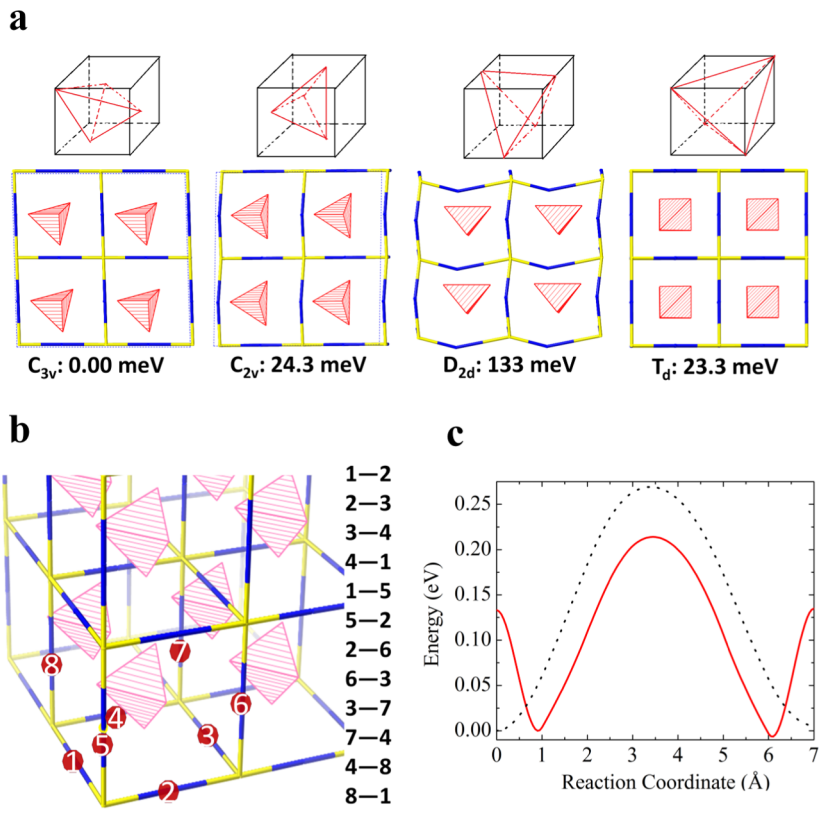

Figure 6. (a) Supercells with four distinctive orientational symmetries, C_{3v}, C_{2v}, D_{2d}, and T_d of BCl_4^- (red tetrahedra) inside the pseudo-cubic cell. The values are the energy per atom relative to the ground-state C_{3v} configuration. (b) 12 possible migration routes between vertices of SNa_6 octahedron. NEB calculations are conducted for each of them for all four cases of BCl_4^- configurations in (a). (c) The averaged profile of migration barrier for the ground state with C_{3v} symmetry (black). Also shown is the averaged migration barrier of our thermodynamic model at 300 K (according to eq 6), taking into account of all four configurations in (a) (red).

conductivity of $Na_3S(BCl_4)_{0.5}I_{0.5}$ is the lower limit among the series $Na_3S(BCl_4)_{0.5}A_{0.5}$ (A = Cl, Br, or I), given that both Cl and Br have larger size difference with BCl_4^- compared to I.

To see that the sodium ions indeed take advantage of the "redundant" space around iodine in $Na_3S(BCl_4)_{0.5}I_{0.5}$, we first equipartition the supercell into eight unit cells centered by either BCl_4^- (called c-cell) or I^- (called I-cell), as shown in Figure 4b. Then, using the AIMD data over 250 ps, we calculate the probability for a Na^+ to move around the cluster ion or the elementary ion by counting the number of sodium ions that fall into the c-cell or the I-cell. We found that the average number of sodium per I-cell is 3.79 vs that for the c-cell is 1.96. Thus, the probability of Na^+ moving around the iodine sites is almost twice as much as that around the cluster sites, which indicates the importance of utilizing the free space around iodine in improving ionic conductivity.

The above results show the following trends from Na_3OBr to $Na_3S(BCl_4)$ to $Na_3S(BCl_4)_{0.5}I_{0.5}$: (i) the anion size and therefore the jumping distance (a_0) of Na^+ is increasing; (ii) the upper limit of phonon frequency and therefore the characteristic Debye frequency is decreasing; (iii) the activation energy (E_a) is decreasing. According to the hopping theory, the prefactor in the Arrhenius relation in eq 3 is

$$A \sim \frac{\sqrt{E_a}}{a_0} \tag{4}$$

Therefore, the prefactors of Na_3OBr, $Na_3S(BCl_4)$, and $Na_3S(BCl_4)_{0.5}I_{0.5}$ should decrease. Indeed, as expected, the calculated prefactors for Na_3OBr, $Na_3S(BCl_4)$, and $Na_3S(BCl_4)_{0.5}I_{0.5}$ are $10^{-4.18}$, $10^{-4.71}$, and $10^{-4.83}$ $(K\cdot cm^2)/s$, respectively. This is known as the "compensation rule", which states that a decreasing activation barrier often coincides with a lower prefactor.[11] Interestingly, the decreasing prefactor here also coincides with the decreasing Debye frequency as in trend (ii). A similar phenomenon is observed in the lithium superionic argyrodites Li_6PS_5X (X = Cl, Br, I), where the prefactor is decreasing due to the lowered Debye frequency and softening of the lattice.[11]

Conduction Mechanism. To understand the conduction mechanism of the new superionic conductor, it is important to study the motion pattern of Na^+ inside the material. Therefore, we have carried out statistical analysis on the MD simulation data using the distinct van Hove time correlation function

$$G_d(r, t) = \frac{1}{N}\langle \sum_{i\neq j}^{N} \delta[r + r_j(0) - r_i(t)]\rangle \tag{5}$$

The function measures the probability of finding, at time t, another ion at distance r_i given the first ion at r_j at $t = 0$. For instance, if, throughout time, distinctive peaks of such probability are observed around distances between Na−Na ion pairs as those in the original crystal structure, it suggests that the motion of Na ions is highly cooperative, the ions maintain their relative positions after steps of hopping.

Such cooperative motion of Na^+ is found in $Na_3S(BCl_4)$. Figure 5a shows the distances between Na−Na pairs in the crystal structure of $Na_3S(BCl_4)$. As shown in Figure 5b, throughout time, the calculated function exhibits distinctive

DOI: 10.1021/acsami.8b19003
ACS Appl. Mater. Interfaces 2019, 11, 963−972

peaks of probability around distances exactly those in the crystal structure. To see the temperature effect on such cooperative motion, the function at 1200 K is also computed, as shown in Figure 5c. The distinctive stripes remain, although they become more diffused. It seems that the cooperative motion of Na^+ is a general character for the Na-rich antiperovskites, as similar behavior is observed in Na_3OBr, as shown in Figure 5d.

An interesting feature of the time correlation function of $Na_3S(BCl_4)$ is that although the distinctive stripes are sustained throughout time, there is a drastic reduction of the probability peaks within a short amount of time (less than 5 ps). This suggests that given their cooperative motion, Na ions in $Na_3S(BCl_4)$ will not stay at their exact lattice sites. Instead, there is high probability for them to be at positions around the original sites, causing a widened and smeared probability stripe around a particular distance. By comparing to the case of Na_3OBr at 1200 K (Figure 5d), such feature is much more prominent in $Na_3S(BCl_4)$, i.e., the probability stripes of $Na_3S(BCl_4)$ at the same temperature are much more smeared.

According to the results mentioned in the former sections, several factors contribute to the high ionic conductivity and low activation energy of $Na_3S(BCl_4)$. These include the small ratio of V_{Na}/CS (Table 1) and the presence of qRUMs with extremely low energy (Figure 2). The presence of sulfur instead of oxygen in the composition serves to first stabilize the antiperovskite structure with the large cluster BCl_4^- (for the requirement of tolerance factor) and second produces weaker interaction with Na^+ compared to oxygen. These factors are "self-consistent". For example, the small V_{Na}/CS ratio also means large room for the cluster ion to rotate and therefore lowers the energy of qRUMs.

We use a simple model with Boltzmann distribution to show that the translation and changing orientation of the tetrahedral cluster BCl_4^- can significantly reduce the migration barrier of Na^+. The model has four distinctive symmetry groups of a tetrahedron in a cubic field: C_{3v}, C_{2v}, D_{2d}, and T_d. Thus, as shown in Figure 6a, there are four possible configurations in which the orientation of BCl_4^- clusters is described by the four symmetries. The averaged migration barrier of Na^+ is then calculated according to

$$\langle E_b \rangle = \frac{\sum_i^4 \langle E_b^i \rangle \cdot \exp(-\varepsilon_i/k_B T) \cdot n_i}{\sum_i^4 \exp(-\varepsilon_i/k_B T) \cdot n_i} \quad (6)$$

where $\exp(-\varepsilon_i/k_B T)$ is the Boltzmann factor and ε_i the energy of the ith configuration, as shown in Figure 6a. n_i is the number of equivalent orientations for each symmetry group: 12, 8, 6, and 2 for C_{3v}, C_{2v}, D_{2d}, and T_d, respectively. For each configuration in Figure 6a, profiles of energy barrier along the 12 possible routes (shown in Figure 6b) are calculated using the NEB method. The cluster ions are allowed to relax when Na^+ ion passes by, lowering the energy barrier. $\langle E_b^i \rangle$ is the averaged migration barrier over the 12 profiles. It is found that for the configurations with symmetries other than C_{3v} (the ground state), there are always significant residual forces on atoms during the NEB calculations, suggesting frustrated energy states around the oriented cluster. A similar structural frustration (i.e., removal of strong lattice site preference) has been reported for $Li_2B_{12}H_{12}$ and $Na_2B_{12}H_{12}$, where large cluster $B_{12}H_{12}^{2-}$ is present.[31] Therefore, we adopt relaxed criteria for NEB convergence with maximal force being smaller than 0.08 eV/Å, corresponding to an energy deviation in the order of 0.001 eV.

The calculated averaged Na migration barrier according to eq 6 is shown (in red) in Figure 6c. Compared with the migration barrier in the ground state (in black) with C_{3v} symmetry, the modeled profile of barrier, taking into account of different orientations of BCl_4^- cluster, has two distinctive features. One is that the energy barrier is significantly reduced from 0.28 eV to about 0.2 eV, which is close to the calculated activation energy (0.17 eV) from AIMD. The second feature is that along the energy profile, the lowest energy position deviates from the original lattice site. This explains the disappearance of strong preference for the Na ions in $Na_3S(BCl_4)$ to stay at the lattice sites, as shown by the smeared probability stripes in Figure 5c.

The above results demonstrate the critical roles of translational and rotational motions of the cluster ions, corresponding to the low-energetic qRUMs, in enabling the high ionic conductivity. Without such motion, the superionic conductivity of the material will disappear, as shown in Figure 7. Similar behavior has also been found in our former studies on cluster-based Li-rich antiperovskites (e.g., Li_3OBH_4).[25] The importance of the low-energetic motions of the cluster ions is not that such motions are coupled with the migration of Na^+ or Li^+, as has been proved in our previous study.[25] Instead, it provides flexibility to the clusters to deviate from their ground-state orientation as well as to move to lower the energy barrier for the passing metal ions. This can significantly lower the Coulombic attraction they exert on the metal ions.[22,25] In other words, instead of serving as "paddle wheels" that "kick" (or attract) the metal ions around, the clusters serve more like "open doors", which allow an easy passage for the metal ions through translation motion and changing orientation.

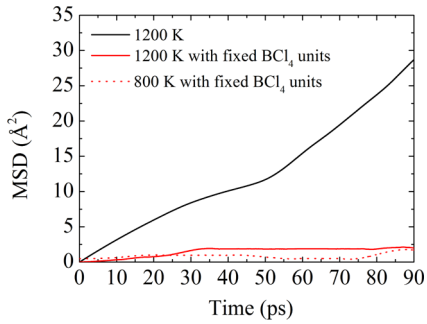

Figure 7. Calculated MSD of Na^+ using data from AIMD simulations. With fixed cluster ions, the superionic conductivity of the material disappears, suggesting the critical role of the motions of the cluster ions on the property.

Mechanical Property. The mechanical property of a superionic conductor is another key factor to consider when forming SIB. Volumes of the electrodes of a SIB are likely to change significantly during the charging−discharging cycle. A good solid electrolyte should be able to elastically deform to accommodate the volume change and maintain a close contact with the electrodes. This is essential to maintain the battery capacity and cycle performance.[32] The elastic constants of a cubic material are proportional to square of the slope of the acoustic branches along certain high symmetry directions in the reciprocal space. Given that $Na_3S(BCl_4)$ has qRUMs with an exceptionally low upper-bound energy, the slope of its acoustic branches, hence the elastic constants are expected to

DOI: 10.1021/acsami.8b19003
ACS Appl. Mater. Interfaces 2019, 11, 963−972

be small. Indeed, like most soft sulfide solid electrolytes with Young's moduli in the range of 18−25 GPa,[32] the calculated Young's modulus and shear modulus of the material are only 21.7 and 13.8 GPa, respectively, as shown in Table 2. The

Table 2. Calculated Elastic constants, Young's modulus (E), Poisson's ratio (ν), and Shear Modulus (μ) (in GPa) of Na_3SBCl_4 with a Pseudo-Cubic Symmetry

c_{11}	41.9
c_{12}	26.2
c_{44}	13.8
E	21.7
ν	0.38
μ	13.8

Poisson's ratio of the material is calculated to be 0.38: a value that falls into the category of metals. These mechanical metrices, in contrast with the large Young's modulus (52 GPa) and small Poisson's ratio (0.22) of Na_3OBr,[23] suggest that $Na_3S(BCl_4)$ can be well densified and is likely to make better contact with the electrodes in a SIB. On the other hand, for a polycrystalline solid electrolyte, large grain size is preferred to enable high ionic conductivity.[30] In this regard, the effect of small elastic constants remains to be seen.

CONCLUSIONS

In this work, we provide a guideline for the rational design of Na-rich antiperovskite superionic conductors with high RT ionic conductivity and low activation energy using cluster ions as building blocks. The conditions cluster ions should meet include: (1) the cluster ion, for the required tolerance factor, should stabilize the antiperovskite structure by coupling with oxygen or sulfur. (2) The cluster ion should create large channel size (CS) and small V_{Na}/CS ratio. (3) The antiperovskite based on the cluster ion should have low-energetic qRUMs, suggesting a softened lattice. This also suggests that more qRUMs can be thermally excited at low and medium temperatures, which can help the Na^+ hopping inside the material. (4) The ionic conductivity of the cluster-based antiperovskite can be further enhanced by forming a mixed phase consisting of both the cluster ion and an elementary ion. The disparity in size between the cluster ion and the elementary ion creates excess volume in the crystal. Together with the cooperative motion of Na^+ found in the material (Figure 5), these are consistent with a more general phenomenon known as "geometric frustration", which is considered as a recipe for high ionic conductivity.[8] According to these guidelines, Na-rich antiperovskite superionic conductors $Na_3S(BCl_4)$ and $Na_3S(BCl_4)_{0.5}I_{0.5}$ based on the cluster ion BCl_4^- are proposed. The extrapolated RT Na^+ conductivity of the materials is above 10^{-3} S/cm. The materials have activation energies smaller than 0.20 eV and large bandgap around 4 eV. The materials can be well densified due to their small elastic moduli and are likely to make good contact with the electrodes.

The stability and formation energy of the cluster-based Na-rich superionic conductor are evaluated, and possible synthesis routes are provided. Moreover, the conduction mechanism of the cluster-based Na-rich antiperovskite is studied. It is found that Na^+ motions inside the material are highly cooperative. We demonstrate that changing the orientation of the tetrahedral cluster ion (corresponding to the thermal excitation of qRUMs) can significantly reduce the migration barrier of Na^+ as well as the strong preference for Na ions to stay at the lattice sites. The current work provides yet another example of cluster ions as building blocks of bulk materials with improved properties.[6,33−38]

METHOD

DFT Calculations. Calculations based on density functional theory (DFT) are carried out to optimize the unit cell of the studied materials using Perdew−Burke−Ernzerhof (PBE) generalized gradient approximation[39] implemented in the VASP package.[40]The projector augmented wave[41] pseudopotential method and 8 × 8 × 8 Monkhorst−Pack k-point mesh are employed in the calculation. The cutoff energy is 550 eV. The energy convergence is set to 10^{-6} eV, and the force convergence is set to 0.005 eV/Å. The van der Waals interaction (as implemented in the DFT + D2 method[42,43]) is considered during the optimization calculations. The Na^+ migration barriers are calculated using the climbing image nudged elastic band method.[44]

Internal Charge Distribution of the Clusters. Bader charge analysis is used to obtain charge distribution of the clusters in the studied crystals.

Lattice Dynamics. The phonon dispersion relations of the studied materials are calculated using the density functional perturbation theory with van der Waals interaction. Geometry of the unit cell is optimized with an energy convergence of 10^{-8} eV and force convergence of 10^{-4} eV/Å. Phonon frequencies are first calculated on a q-grid of 5 × 5 × 5. Frequencies for other q points are then interpolated from the calculated points.

qRUMs of Na-Rich Antiperovskites. The qRUMs of the studied materials are obtained by mapping the phonon eigenvectors of a model system containing rigid cluster ions to the eigenvectors of the studied system. The model system is created and calculated using an improved version of the CRUSH code.[45,46]

Thermodynamics and Superionic Conductivity. Ab initio molecular dynamics (AIMD) simulations are performed. An NPT ensemble is used to study the thermodynamics of the materials at 400 and 600 K under ambient pressure, using a 3 × 3 × 3 supercell and 1.0 fs time step. To study the Na^+ transport, AIMD simulations with 2.0 fs time step and NVT ensemble are carried out at different temperatures using a 2 × 2 × 2 supercell with one Na^+ vacancy to speed up the ion-hopping process. At each temperature, the AIMD simulation lasts over 250 ps (i.e., 125 000 time steps given each time step of 2.0 fs = 0.002 ps) after a 40 ps pre-equilibrium run to make the linear fit to the averaged mean square displacement (MSD) of Na^+ converge. The diffusion coefficient (D) at each temperature is calculated by fitting to the MSD according to

$$D = \lim_{t\to\infty}\left[\frac{1}{6t}\langle[\mathrm{r}\rightarrow(t)]^2\rangle\right] \quad \text{(m1)}$$

with $r \rightarrow (t)$ being the displacement of Na^+ at time t. The conductivity (σ) is then calculated from the Nernst−Einstein relation

$$\sigma = D\frac{Ne^2}{kT} \quad \text{(m2)}$$

DOI: 10.1021/acsami.8b19003
ACS Appl. Mater. Interfaces 2019, 11, 963−972

with N being the number of ions per cm^3. Other symbols have their customary meaning. The activation energy E_a is obtained by using the Arrhenius model

$$\sigma = \frac{A}{T}\exp\left(\frac{E_a}{kT}\right) \quad \text{(m3)}$$

where A and E_a are fitting parameters. k and T are the Boltzmann constant and the temperature, respectively.

Elastic Constants. Elastic tensors are computed using the VASP code. The Young's modulus (E), shear modulus (μ), and the Poisson's ratio (υ) are calculated as

$$E = \frac{c_{11}^2 + c_{12}c_{11} - 2c_{12}^2}{c_{11} + c_{12}} \quad \text{(m4)}$$

$$\mu = c_{44} \quad \text{(m5)}$$

$$\upsilon = \frac{c_{12}}{c_{11} + c_{12}} \quad \text{(m6)}$$

AUTHOR INFORMATION

Corresponding Author

*E-mail: pjena@vcu.edu.

ORCID

Hong Fang: 0000-0002-0968-8687

Puru Jena: 0000-0002-2316-859X

Notes

The authors declare no competing financial interest.

ACKNOWLEDGMENTS

The work is supported in part by the U.S. Department of Energy, Office of Basic Energy Sciences, Division of Materials Sciences and Engineering under Award No. DE-FG02-96ER45579. Resources of the National Energy Research Scientific Computing Center supported by the Office of Science of the U.S. Department of Energy under Contract no. DE-AC02-05CH11231 are also acknowledged.

REFERENCES

(1) Hwang, J. Y.; Myung, S.; Sun, Y. Sodium-Ion Batteries: Present and Future. *Chem. Soc. Rev.* **2017**, *46*, 3529−3614.

(2) Zhang, L.; Yang, K.; Mi, J.; Lu, L.; Zhao, L.; Wang, L.; Li, Y.; Zeng, H. Solid Electrolytes Na_3PSe_4: A Novel Chalcogenide Solid Electrolyte with High Ionic Conductivity. *Adv. Energy Mater.* **2015**, *5*, No. 1501294.

(3) Wenzel, S.; Leichtweiss, T.; Weber, D. A.; Sann, J.; Zeier, W. G.; Janek, J. Interfacial Reactivity Benchmarking of the Sodium Ion Conductors Na_3PS_4 and Sodium β-Alumina for Protected Sodium Metal Anodes and Sodium All-Solid-State Batteries. *ACS Appl. Mater. Interfaces* **2016**, *8*, 28216−28224.

(4) Guin, M.; Tietz, F. Survey of the Transport Properties of Sodium Superionic Conductor Materials for Use in Sodium Batteries. *J. Power Sources* **2015**, *273*, 1056−1064.

(5) Braga, M. H.; Murchison, A. J.; Ferreira, J. A.; Singh, P.; Goodenough, J. B. Glass-Amorphous Alkali-Ion Solid Electrolytes and Their Performance in Symmetrical Cells. *Energy Environ. Sci.* **2016**, *9*, 948−954.

(6) Tang, W. S.; Matsuo, M.; Wu, H.; Stavila, V.; Zhou, W.; Talin, A. A.; Soloninin, A. V.; Skoryunov, R. V.; Babanova, O. A.; Skripov, A. V.; Unemoto, A.; Orimo, S.-I.; Udovic, T. J. Liquid-Like Ionic Conduction in Solid Lithium and Sodium Monocarba-closo-Decaborates Near or at Room Temperature. *Adv. Energy Mater.* **2016**, *6*, No. 1502237.

(7) Zhang, Z.; Ramos, E.; Lalere, F.; Assoud, A.; Kaup, K.; Hartman, P.; Nazar, F. $Na_{11}Sn_2PS_{12}$: a New Solid State Sodium Superionic Conductor. *Energy Environ. Sci.* **2018**, *11*, No. 87.

(8) Düvel, A.; Heitjans, P.; Fedorov, P.; Scholz, G.; Cibin, G.; Chadwick, A. V.; Pickup, D. M.; Ramos, S.; Sayle, L. W. L.; Sayle, E. K. L.; Sayle, T. X. T.; SayleIs, D. C. Geometric Frustration-Induced Disorder a Recipe for High Ionic Conductivity? *J. Am. Chem. Soc.* **2017**, *139*, 5842−5848.

(9) Song, A.-Y.; Xiao, Y.; Turcheniuk, K.; Upadhya, P.; Ramanujapuram, A.; Benson, J.; Magasinski, A.; Olguin, M.; Meda, L.; Borodin, O.; Yushin, G. Protons Enhance Conductivities in Lithium Halide Hydroxide/Lithium Oxyhalide Solid Electrolytes by Forming Rotating Hydroxy Groups. *Adv. Energy Mater.* **2018**, *8*, No. 1700971.

(10) Dawson, J. A.; Attari, T. S.; Chen, H.; Emge, S. P.; Johnston, K. E.; Islam, M. S. Elucidating Lithium-Ion and Proton Dynamics in Anti-perovskite Solid Electrolytes. *Energy Environ. Sci.* **2018**, *11*, 2993−3002.

(11) Kraft, M. A.; Culver, S. P.; Calderon, M.; Böcher, F.; Krauskopf, T.; Senyshyn, A.; Dietrich, C.; Zevalkink, A.; Janek, J.; Zeier, W. G. Influence of Lattice Polarizability on the Ionic Conductivity in the Lithium Superionic Argyrodites Li_6PS_5X (X = Cl, Br, I). *J. Am. Chem. Soc.* **2017**, *139*, 10909−10918.

(12) Richards, W. D.; Wang, Y.; Miara, L. J.; Kim, J. C.; Ceder, G. Design of $Li_{1+2x}Zn_{1-x}PS_4$, a New Lithium Ion Conductor. *Energy Environ. Sci.* **2016**, *9*, 3272−3278.

(13) Sun, Y.; Suzuki, K.; Hori, S.; Hirayama, M.; Kanno, R. Superionic Conductors: $Li_{10+\delta}[Sn_ySi_{1-y}]_{1+\delta}P_{2-\delta}S_{12}$ with a $Li_{10}GeP_2S_{12}$-type Structure in the Li_3PS_4−Li_4SnS_4−Li_4SiS_4 Quasi-Ternary System. *Chem. Mater.* **2017**, *29*, 5858−5864.

(14) Kaup, K.; Lalere, F.; Hup, A.; Shyamsunder, A.; Adermann, T.; Hartmann, P.; Nazar, L. F. Correlation of Structure and Fast Ion Conductivity in the Solid Solution Series $Li_{1+2x}Zn_{1-x}PS_4$. *Chem. Mater.* **2018**, *30*, 592−596.

(15) Li, Y.; Zhou, W.; Xin, S.; Li, S.; Zhu, J.; Lî, X.; Cui, Z.; Jia, Q.; Zhou, J.; Zhao, Y.; Goodenough, J. B. Fluorine-Doped Antiperovskite Electrolytes for All-Solid-State Lithium-Ion Batteries. *Angew. Chem., Int. Ed.* **2016**, *55*, 965−9968.

(16) Sagotra, A. K.; Cazorla, C. Stress-Mediated Enhancement of Ionic Conductivity in Fast-Ion Conductors. *ACS Appl. Mater. Interfaces* **2017**, *9*, 38773−38783.

(17) Zhu, Z.; Chu, I.-H.; Deng, Z.; Ong, S. P. Role of Na^+ Interstitials and Dopants in Enhancing the Na^+ Conductivity of the Cubic Na_3PS_4 Superionic Conductor. *Chem. Mater.* **2015**, *27*, 8318−8325.

(18) Wang, Y.; Wang, Q.; Liu, Z.; Zhou, Z.; Li, S.; Zhu, J.; Zou, R.; Wang, Y.; Lin, J.; Zhao, Y. Structural Manipulation Approaches Towards enhanced Sodium Ionic Conductivity in Na-rich Antiperovskites. *J. Power Sources* **2015**, *293*, 735−740.

(19) Zhao, Y.; Wang, Y.; Zou, R. Sodium Anti-perovskite Solid Electrolyte Compositions. WO Application WO2016026130A1, 2016.

(20) Zhu, J.; Wang, Y.; Li, S.; Howard, J. W.; Neuefeind, J.; Ren, Y.; Wang, H.; Liang, C.; Yang, W.; Zou, R.; Jin, C.; Zhao, Y. S. Sodium Ion Transport Mechanisms in Antiperovskite Electrolytes Na_3OBr and Na_4OI_2: An *in Situ* Neutron Diffraction Study. *Inorg. Chem.* **2016**, *55*, 5993−5998.

(21) Dawson, J. A.; Chen, H.; Islam, M. S. Composition Screening of Lithium- and Sodium-Rich Anti-Perovskites for Fast-Conducting Solid Electrolytes. *J. Phys. Chem. C* **2018**, *122*, 23978−23984.

(22) Fang, H.; Jena, P. Li-Rich Antiperovskite Superionic Conductors based on Cluster Ions. *Proc. Natl. Acad. Sci. U.S.A.* **2017**, *114*, 11046−11051.

(23) Ramanna, J.; Yedukondalu, N.; Babu, K. R.; Vaitheeswaran, G. *Ab Initio* Study of Electronic Structure, Elastic and Optical Properties of Anti-perovskite Type Alkali Metal Oxyhalides. *Solid State Sci.* **2013**, *20*, 120−126.

(24) Kieslich, G.; Sun, S.; Cheetham, A. K. An Extended Tolerance Factor Approach for Organic−Inorganic Perovskites. *Chem. Sci.* **2015**, *6*, 3430−3433.

DOI: 10.1021/acsami.8b19003
ACS Appl. Mater. Interfaces 2019, 11, 963−972

(25) Fang, H.; Wang, S.; Liu, J.; Sun, Q.; Jena, P. Superhalogen-Based Lithium Superionic Conductors. *J. Mater. Chem. A.* **2017**, *5*, 13373−13381.
(26) Cazorla, C.; Sagotra, A. K.; King, M.; Errandonea, D. High-Pressure Phase Diagram and Superionicity of Alkaline Earth Metal Difluorides. *J. Phys. Chem. C* **2018**, *122*, 1267−1279.
(27) Cazorla, C.; Alfe, D.; Gillan, M. J. Constraints on the Phase Diagram of Molybdenum from First-Principles Free-Energy Calculations. *Phys. Rev. B* **2012**, *85*, No. 064113.
(28) Ott, K. C. *Final Report for the DOE Chemical Hydrogen Storage Center of Excellence*, LA-UR-20074; Los Alamos National Lab, 2010; p 13.
(29) Che, H.; Chen, S.; Xie, Y.; Wang, H.; Amine, K.; Liao, X.; Ma, Z. Electrolyte Design Strategies and Research Progress for Room-Temperature Sodium-Ion Batteries. *Energy Environ. Sci.* **2017**, *10*, 1075−1101.
(30) Dawson, J. A.; Canepa, P.; Famprikis, T.; Masquelier, C.; Islam, M. S. Atomic-Scale Influence of Grain Boundaries on Li-Ion Conduction in Solid Electrolytes for All-Solid-State Batteries. *J. Am. Chem. Soc.* **2018**, *140*, 362−368.
(31) Kweon, K. E.; Varley, J. B.; Shea, P.; Adelstein, N.; Mehta, P.; Heoo, T. W.; Udovic, T. J.; Stavila, V.; Wood, B. C. Structural, Chemical, and Dynamical Frustration: Origins of Superionic Conductivity in Closo-Borate Solid Electrolytes. *Chem. Mater.* **2017**, *29*, 9142−9153.
(32) Sakuda, A.; Hayashi, A.; Tatsumisago, M. Sulfide Solid Electrolyte with Favorable Mechanical Property for All-Solid-State Lithium Battery. *Sci. Rep.* **2013**, *3*, No. 2261.
(33) Fang, H.; Jena, P. Super-Ion Inspired Colorful Hybrid Perovskite Solar Cells. *J. Mater. Chem. A* **2016**, *4*, 4728−4737.
(34) Fang, H.; Jena, P. Atomic-Level Design of Water-Resistant Hybrid Perovskites for Solar Cells by Using Cluster Ions. *J. Phys. Chem. Lett.* **2017**, *8*, 3726−3733.
(35) Fang, H.; Jena, P. B_{12} $(SCN)_{12}^{2-}$: An Ultrastable Weakly Coordinating Dianion. *J. Phys. Chem. C* **2017**, *121*, 7697−7702.
(36) Zhong, M.; Fang, H.; Jena, P. $B(SCN)_4^-$: A New Weakly Coordinating Anion in the Tetracyanoborate Family. *J. Phys. Chem. C* **2018**, *122*, 13371−13375.
(37) Yu, C.; Ganapathy, S.; de Klerk, N. J. J.; van Eck, E. R. H.; Wagemaker, M. Na-Ion Dynamics in Tetragonal and Cubic Na_3PS_4, a Na-Ion Conductor for Solid State Na-Ion Batteries. *J. Mater. Chem. A* **2016**, *4*, 15095−15105.
(38) Kaus, M.; Guin, M.; Yavuz, M.; Knapp, M.; Tiet, F.; Guillon, O.; Ehrenberg, H.; Indris, S. Fast Na^+ Ion Conduction in NASICON-Type $Na_{3.4}Sc_2(SiO_4)_{0.4}(PO_4)_{2.6}$ Observed by ^{23}Na NMR Relaxometry. *J. Phys. Chem. C* **2017**, *121*, 1449−1454.
(39) Perdew, J. P.; Burke, K.; Ernzerhof, M. Generalized Gradient Approximation Made Simple. *Phys. Rev. Lett.* **1996**, *77*, No. 3865.
(40) Kresse, G.; Furthmueller, J. Efficiency of *Ab-Initio* Total Energy Calculations for Metals and Semiconductors Using a Plane-Wave Basis Set. *J. Comput. Mater. Sci.* **1996**, *6*, 15−50.
(41) Kresse, G.; Furthmueller, J. Efficient Iterative Schemes for *Ab Initio* Total-Energy Calculations Using a Plane-Wave Basis Set. *Phys. Rev. B* **1996**, *54*, 11169−11186.
(42) Grimme, S. Semiempirical GGA-Type Density Functional Constructed with a Long-Range Dispersion Correction. *J. Comput. Chem.* **2006**, *27*, 1787−1799.
(43) Fang, H.; Dove, M.; Refson, K. Ag-Ag Dispersive Interaction and Physical Properties of $Ag_3Co(CN)_6$. *Phys. Rev. B* **2014**, *90*, No. 054302.
(44) http://theory.cm.utexas.edu.vtsttools/neb.
(45) Giddy, A. P.; Dove, M.; Pawley, G. S.; Heine, V. The Determination of Rigid Unit Modes as Potential Soft Modes for Displacive Phase Transitions in Framework Crystal Structures. *Acta Crystallogr. A* **1993**, *49*, 697−703.
(46) Hammonds, K. D.; Dove, M.; Giddy, A. P.; Heine, V. CRUSH: A FORTRAN Program for the Analysis of the Rigid Unit Mode Spectrum of a Framework Structure. *Am. Mineral.* **1994**, *79*, 1207−1209.

DOI: 10.1021/acsami.8b19003
ACS Appl. Mater. Interfaces 2019, 11, 963−972